Journal of Nuclear Materials 392 (2009) 235–242

Contents lists available at ScienceDirect

Journal of Nuclear Materials

journal homepage: www.elsevier.com/locate/jnucmat

Corrosion of high temperature metallic materials in VHTR

C. Cabet *, F. Rouillard

CEA, DEN, DPC, SCCME, Laboratoire d'Etude de la Corrosion Non Aqueuse, F-91191 Gif-sur-Yvette, France

A B S T R A C T

Helium coolant of High Temperature Reactors is expected to contain impurities which can interact with structural nickel base metallic materials at elevated temperatures. A continuous, self-healing, chromia-based surface scale is needed to act as a barrier against the reactive gasses. However in specific operational conditions, a process occurs at high temperature which irreversibly reduces the chromia layer. The unprotected alloy can then suffer from deleterious corrosion phenomena, such as carburization or decarburization, which can significantly impact the mechanical stability. First, control of the helium chemistry can be used to mitigate the high temperature corrosion of nickel base alloys by suppressing the chromia reduction reaction. Optimization of the alloy composition is a further solution as chromia forming alloys exhibit different oxidation rates in relation to their content of minor reactive elements. Data published on Alloy 617 and Alloy 230 is reviewed in the present paper.

1. Introduction

Based on the High Temperature Reactor technology (HTR), the Very High Temperature Reactor (VHTR) is considered to be the nearest term Next Generation Nuclear Plant (NGNP) [1]. It is a helium cooled reactor fuelled by TRISO-coated particles [2]. VHTR with a thermal neutron spectrum uses an all-graphite core, either as solid blocks or as a pebble bed. In order to achieve high efficiency energy conversion or thermochemical production of hydrogen, the temperature of the cooling gas has to be as high as possible. The targeted helium outlet temperature is between 1123 and 1223 K. Helium flows through a structural duct (hot gas duct) then an intermediate heat exchanger (IHX), which will divert heat from the primary side of the system to a secondary fluid, and returns into the Reactor Pressure Vessel at about 663–763 K. The IHX that isolates the primary and secondary circuits must resist a pressure differential of 6–7 MPa during off-normal events. As compact IHXs are required, the component walls have to be thin (order of magnitude is mm). In addition, the system seeks long service lifetimes, about 20 years for the IHX. These conditions are beyond today's nuclear applications (ASME codes for nuclear reactor materials reach only about 1035 K) and will challenge the structural materials. Prime candidate systems are high temperature metallic materials [3]; to meet the desired temperatures, pressures and lifetimes, these alloys must be thermally stable, creep resistant and compatible with the coolant.

This paper reviews published data [4–11] that deal with the corrosion resistance of candidate high temperature metallic alloys, Alloys 617 and 230, in the specific environment of the reactor primary circuit. It is shown that the reactive impurities H_2O, CO, H_2, and CH_4 in the cooling gas interact with Ni alloys at high temperature causing corrosion effects that can significantly influence the in-depth microstructure, and consequently the mechanical properties.

2. High temperature materials and reactor environment

2.1. High temperature alloys

Past R&D programs in support of the development of HTR plants (eg DRAGON, Peach Bottom, AVR, THTR, Fort St Vrain...) performed an early selection of high temperature metallic materials. Considering the temperature operating range of 663–1123 K and possibly 1223 K, structural stability, resistance to creep and high temperature oxidation are the most determining properties. Alloy 800 type alloys were considered for intermediate temperatures (up to 1033 K) and wrought creep resistant Ni base alloys for the highest temperatures [12]. Hastelloy X was said to exhibit good corrosion behavior in helium coolant at least up to about 1173 K and variants XR and XR2 were manufactured in Japan to further improve the oxidation resistance [13]. Alloy 617, strengthened by addition of Co and Mo, was observed to be the most creep resistant of all tested materials [14]. Over the last 20 years, other alloys have been developed for high temperature applications that could be appropriate IHX and circuit materials. In particular Alloy 230 associates high thermal stability and mechanical strength (strengthening by addition of W, approx. 14 wt%) with good oxidation properties (minor addition of La, approx. 0.02 wt%, improves the corrosion resistance via the so-called reactive element effect) [15].

* Corresponding author. Tel.: +33 169 08 16 15; fax: +33 169 08 15 86.
E-mail address: celine.cabet@cea.fr (C. Cabet).

0022-3115/$ - see front matter © 2009 Elsevier B.V. All rights reserved.
doi:10.1016/j.jnucmat.2009.03.029

All previous alloys contain a high chromium weight fraction, around 20–22 wt%, for oxidation resistance: at elevated temperatures, they are able to form a dense and continuous Cr-rich oxide on their surface. Provided that it grows slowly, the scale provides protection against reactive species.

2.2. Special characteristics of HTR helium

Coolant will be contaminated by impurities from a variety of sources. Graham et al. [16] listed these sources for conventional HTRs, part of which should still be relevant for advanced HTRs: air from charge/discharge of fuel elements; water vapor (and carbon oxides) from the degassing of the core graphite and insulators or from direct inleakages; hydrogen from proton diffusion through materials of water-cooled heat exchangers and coolers. The primary impurities react with the large volumes of hot graphite: virtually all free oxygen is removed to form CO; H_2O is only partly converted to H_2 and CO; any CO_2 is also largely reduced to CO; radiolytic reaction of H_2 with graphite at intermediate temperature produces some CH_4; CH_4 then dissociates on hotter surfaces. A purification system will continuously treat part of the total coolant flow to decrease the global impurity levels and controlled injection of species is considered to control the gas chemistry. Impurities circulating in the primary circuit helium thus result from a dynamic balance between impurity inputs (as contamination and controlled injection), purification efficiency and in situ reactions, driven by the hot graphite. Due to short dwell times as well as low impurity contents, the gas phase does not reach thermodynamic equilibrium, but helium chemistry was shown to reach a steady state composition [17]. The main impurities in an advanced HTR primary circuit helium are expected to be H_2, H_2O, CO, CH_4, N_2, and possibly CO_2 [16–20]. Actual levels in a given system will be dependent on the detailed design and construction features (purification ratio, core temperature, graphite type...). For instance, the German PNP program used a standard test helium with 50 Pa H_2, 1.5 Pa CO, 2 Pa CH_4, 0.15 Pa H_2O and up to 0.5 Pa N_2 [21].

2.3. Gas/metal surface reactions

Although at very low contents, the helium impurities interact with high temperature metallic materials. In highly diluted helium, reactions independently take place and can only involve a single gas species [22]. The reactivity will be determined by kinetics of the different reactions that transfer C and O to the metallic surface [22–24]:

- Oxidation of a metal M by the *water vapor*

$$xH_2O_{(g)} + M_{(s)} = MO_{x(s)} + x/2H_{2(g)} \quad (1)$$

- Reaction of the *water vapor* with carbon from the alloy

$$H_2O_{(g)} + C_{(s)} \rightarrow CO_{(g)} + H_{2(g)} \quad (2)$$

- Decomposition of the carbon monoxide

$$xCO_{(g)} + M_{(s)} \rightarrow MO_{x(s)} + xC_{(s)} \quad (3)$$

- Decomposition of the methane on the metallic surface

$$CH_{4(g)} = C_{(s)} + 2H_{2(g)} \quad (4)$$

- Reduction of metallic oxide by the methane

$$xCH_{4(g)} + MO_{x(s)} \rightarrow xCO_{(g)} + 2xH_{2(g)} + M_{(s)} \quad (5)$$

$M_{(s)}$ is a metal of the alloy that can be oxidized at the low oxygen potential prevailing in the coolant helium such as Cr, Al, Si, Ti, Mn... and MO_x is the corresponding oxide.

Cr is obviously the key element regarding corrosion of chromia-former alloys. The challenge in HTR helium will be to enable the formation and slow growth of the chromia scale that means that Eq. (1) and (3) to a lesser extend, must occur and overcome all other reactions.

3. Experimental

3.1. Materials

Table 1 reports the chemical composition of the tested alloys.

The as-received and aged microstructure was investigated by TEM [15]. The as-received Alloy 230 contains large intragranular tungsten-rich carbides of the MC_6 type (mean diameter: 5 μm); few smaller $M_{23}C_6$ carbides are also detected along grain boundaries. Ageing at 1223 K causes significant precipitation of secondary carbides at grain boundaries and around primary carbides [10,15]. These secondary carbides are Cr-rich and of the $M_{23}C_6$ type. The as-received Alloy 617 exhibits various populations of carbides: MC (rich in Ti), several types of M_6C (rich in Mo) and several types of $M_{23}C_6$ (rich in Cr). Ageing at 1223 K induced dissolution of small primary carbides and coarsening of larger primary carbides as well as precipitation of secondary Cr-rich $M_{23}C_6$ [15].

Specimens were machined as 25 × 12 mm coupons with a thickness of 0.8–2 mm, polished down to 1 μm alumina powder and ultrasonically degreased in an acetone–ethanol mixture.

3.2. Test loop

Coupons were exposed to flowing impure helium in high temperature quartz tube furnaces (tube inner diameter 116 mm) at atmospheric pressure. The specimen holder and the thermocouple sheath (type-S thermocouple) are also made of quartz, an inert material in the given temperature range. The loop is made of stainless steel pipe with an electronic-grade polish and gas-tight fittings. Before each experiment, all circuits were evacuated, and then flushed with pure helium until the impurity content was below the detection limit of the analyzers. A main flow of research-grade helium is in-line purified through gas cartridges (GASKEEPER™), and residual water vapor is further reduced via a cryogenic trap (163 K). Then mass flow controllers meter impurities into helium from He/CH_4, He/H_2, and He/CO gas cylinders (contaminants are removed from the He/CH_4 and He/H_2 mixtures using purification cartridges). Water vapor is finally added by mass flow controllers from purified then moistened helium (saturation in vapor through de-aerated water at 275 K). Helium composition is analyzed at the test-section inlet and outlet by gas phase chromatography (He detector; detection limit: 0.01 Pa). In any case, oxygen and carbon dioxide partial pressures are below the chromatography detection limit; nitrogen is below 0.5 Pa. Water vapor partial pressure is monitored on-line via a capacitive-probe hygrometer coupled to a high-sensitivity chilled-mirror dew-point analyzer.

Blank tests were carried out without any specimen in order to check that the loop and specimen holder materials do not significantly react with gaseous impurities, or influence the gas composition.

3.3. Test conditions

Table 2 gives the impurity concentrations and water vapor content of the test gas mixtures; these compositions are close to those expected in VHTR coolant helium. Equivalent partial pressure of oxygen Po_2^{eq} is also tentatively proposed in the Table; the calculation considers the equilibrium conditions for water vapor dissociation at 1173 K with the prevailing partial pressures of hydrogen and water vapor in helium.

Table 1
Chemical composition of alloys (wt%).

	Ni	Cr	C	W	Co	Mo	Fe	Al	Mn	Ti	Si	La	B
Alloy 617	base	21.6	0.06	–	12.0	9.2	1.0	1.0	0.1	0.4	0.2	~0.02	0.002
Alloy 230	base	22.0	0.10	14.7	0.2	1.3	1.3	0.4	0.5	0.1	0.4		0.002

Table 2
Composition of the test helium mixtures: He-1 to He-8 for surface reactivity studies (measured critical temperatures T_A in right hand side column) and He-9 to He-12 for corrosion tests; the equivalent partial pressure of oxygen Po_2^{eq} was tentatively calculated considering the equilibrium conditions for the reaction of water vapor dissociation at 1173 K with the $P(H_2)$ and $P(H_2O)$ from second and third columns.

	H_2 (Pa)	H_2O (Pa)	Po_2^{eq} (Pa)	CO (Pa)	CH_4 (Pa)	T_A (K)
He-1	20.5 ± 0.4	0.50 ± 0.24	1.0×10^{-14}	0.61 ± 0.01	2.00 ± 0.04	1168 ± 5
He-2	49.6 ± 0.9	0.20 ± 0.09	2.8×10^{-16}	1.74 ± 0.04	31.0 ± 0.6	1198 ± 5
He-3	19.8 ± 0.4	0.08 ± 0.04	2.8×10^{-16}	2.24 ± 0.04	2.11 ± 0.04	1211 ± 5
He-4	19.3 ± 0.4	0.16 ± 0.08	1.2×10^{-15}	4.90 ± 0.10	1.90 ± 0.04	1236 ± 5
He-5	19.5 ± 0.4	0.40 ± 0.19	7.2×10^{-15}	4.90 ± 0.10	2.10 ± 0.04	1234 ± 5
He-6	18.8 ± 0.4	0.15 ± 0.07	1.1×10^{-15}	5.03 ± 0.10	2.02 ± 0.04	1236 ± 5
He-7	19.6 ± 0.4	0.05 ± 0.02	1.2×10^{-16}	5.25 ± 0.10	2.11 ± 0.04	1242 ± 5
He-8	18.9 ± 0.4	0.06 ± 0.03	1.7×10^{-16}	5.44 ± 0.10		1247 ± 5
He-9	20	0.05–1	2.1×10^{-16}	5	2	
He-10	20	0.05–1.2	2.8×10^{-16}	0.5		
He-11	20	0.05	1.1×10^{-16}	0.5	2	
He-12	50	0.05	1.7×10^{-17}	1.5	30	

For studies on the surface reactivity of alloys, the test gasses He-1 to He-8 are used. Two identical specimens are exposed to a gas flow rate of about 0.2 cm^3/s per cm^2 of metallic surface. Adapted from Ref. [25], the heat treatment involves:

- step 1: heating to 1173 K at 1 K/min and hold at 1173 K for 25 h under impure helium,
- step 2: heating to 1253 K at 0.5 K/min and hold at 1253 K for 20 h under impure helium,
- cooling: natural cooling under pure helium.

The *isothermal corrosion tests* are carried out at 1223 K for different times up to 5000 h under test helium He-9 to He-12 (see Table 2); specimens are heated up at 1 K/min and cooled down at 7.5 K/min in pure helium. The gas flow rate is about 0.1 $cm^3\,s^{-1}$ per cm^2 of metallic surface.

3.4. Techniques of observation and analysis

Analyses and observations of as-received, aged and corroded specimens involve weighing, X-Ray Diffraction (XRD with Co Kα radiation), Glow Discharge Optical Emission Spectroscopy (GDOES) – calibration uses metallic standards for a quantitative analysis of the carbon, Glow Discharge Mass spectrometry (GDMS), measurement of the global carbon content by LECO analyzer, Scanning Electron Microscopy (SEM), Field Emission Scanning Electron Microscopy (FESEM), Energy-Dispersive X-ray spectroscopy (EDX), microprobe (WDS) and Transmission Electron Microscopy (TEM).

4. High temperature reactivity of Ni-base alloys in coolant helium

Reactivity of chromia forming alloys in high temperature impure helium will be illustrated through the description of the behavior of Alloy 230 but similar studies were carried out for other materials such as Hastelloy X and XR, Alloy 617, and Alloy 800H [21,22,24–28].

4.1. Reactivity at intermediate temperature

In step 1 (see Section 3.3), two specimens of Alloy 230 are heated to 1173 K, and then maintained at this temperature under impure helium for 25 h. Fig. 1 shows the gas phase analysis at the furnace outlet during the test. Upon heating, the curve for CO(g) exhibits a negative peak starting at approx. 1073 K which increases as long as the temperature increases; during the isothermal exposure for 25 h, the P(CO) progressively returns to its initial level. This peak corresponds to a consumption of CO(g). In the mean time, the CH_4(g) content barely changes at the furnace outlet.

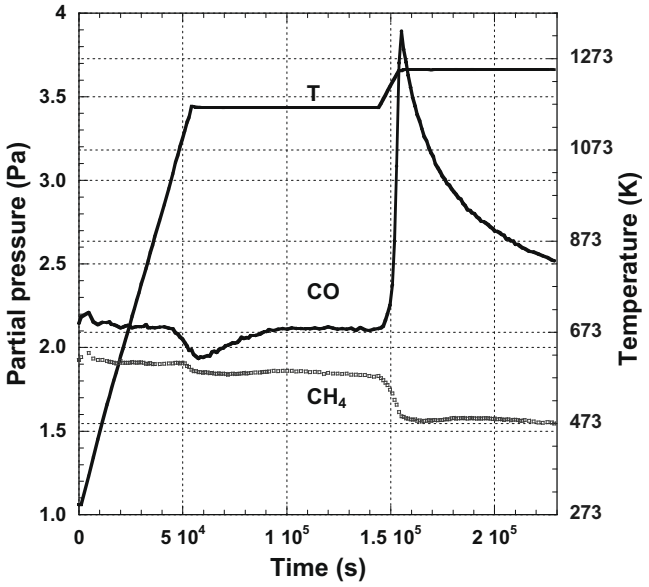

Fig. 1. Temperature program and outlet partial pressure of CO and CH_4 as a function of time – Reactivity of Alloy 230 in He-3.

Fig. 2(a) shows the surface of Alloy 230 after step 1. A continuous, about 1 μm-thick, surface oxide scale has formed; it is made of a chromium-rich oxide that contains manganese in its outer part. Nodules of Si- and Al-rich oxides are also evidenced at the scale/alloy interface, as well as intergranular oxidation of aluminium up to 10 μm deep in the alloy (not visible on the displayed SEM photo). Oxidation of the alloy may result from reactions with two oxidizing species: water vapor and carbon monoxide following Eqs. (1) and (3), with $M_{(s)}$ being mainly Cr but also Al, Mn, Si to a lesser extent.

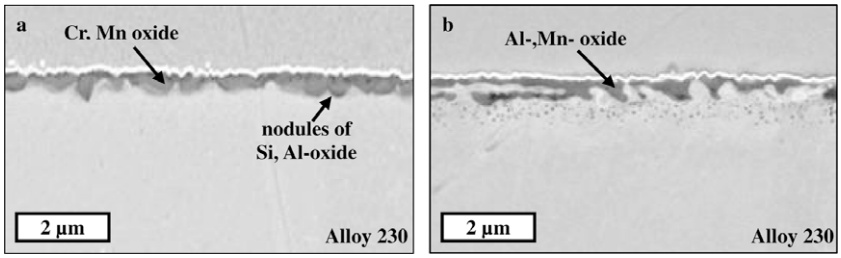

Fig. 2. FESEM images with backscattered electron contrast at 20 kV – Cross section of the Alloy 230 surface after step 1 (a) and after step 2 (b) in He-4.

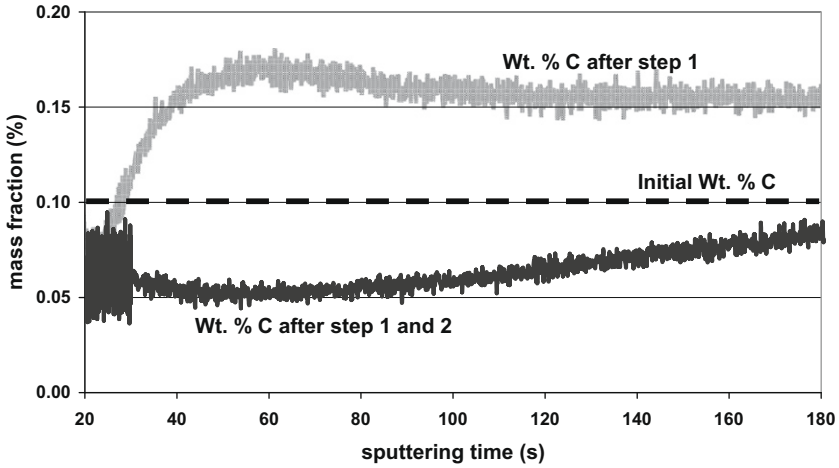

Fig. 3. GDOES profile of carbon at the Alloy 230 surface after step 1 and after step 2 in He-4 (surface is on the left hand side and alloy bulk on the right hand side).

The CO(g) consumption in step 1 is related to Eq. (3) and the total amount of reacted CO(g) can be calculated from Fig. 1. It was shown [7,8] that (i) at the beginning, both CO(g) and H_2O(g) take part in the oxidation process, (ii) the reaction rate of CO(g) continuously decreases until it becomes negligible after about 15 h at 1173 K, (iii) the higher P(H_2O) in helium, the more H_2O(g) reacts and the less CO(g) reacts. Thermodynamic calculation indicates that H_2O has a greater affinity for metals than CO. Nevertheless at 1173 K, CO can react with Al and Si, and with Cr as well if the chromium activity is high enough. It is assumed that oxidation by CO stops (or reaches a negligible value) because Al, Si and Cr may be depleted in the surface vicinity. As a matter of fact, water vapor is the only impurity that takes a significant part in oxidation for long times.

Fig. 3 shows the GDOES carbon profile at the alloy surface after step 1: carbon accumulates underneath the surface oxide. Based on the sputtering rate, carbon has diffused over a distance of more than 20 µm into the alloy. Calculation of the excess carbon, based on the curve in Fig. 3, is in good agreement with the amount of deposited carbon by the CO(g) dissociation as evaluated from Fig. 1; it is thus verified that the increase in carbon content in the alloy comes from the gas phase according to Eq. (3) and that contribution of Eq. (4) is negligible.

4.2. Reactivity at higher temperature

After the oxidation step at 1173 K for 25 h in impure helium, the alloy undergoes a second step: it is heated to 1253 K, maintained for 20 h and then cooled under pure helium. Gas-phase analysis in Fig. 1 shows a sharp increase in the carbon monoxide partial pressure, starting at 1210 ± 5 K. The CO(g) production then decreases while the temperature is kept constant at 1253 K. To a smaller extent, the methane partial pressure concurrently decreases. This CH_4(g) consumption, being associated with a stoichiometric production of H_2(g), can be attributed to reaction between H_2O(g) and CH_4(g) on the metal surface following:

$$H_2O_{(g)} + CH_{4(g)} \overset{\text{metal}}{\rightarrow} CO_{(g)} + 3H_{2(g)} \quad (6)$$

It is noteworthy that the CO(g) peak in Fig. 1 is far too high to be entirely due to Eq. (6) [Eq. (6) may barely account for maximum 10% of the reacted CO(g)].

Tests carried out in a thermobalance demonstrate that the scale does not spall during or after cooling [29]. However, Fig. 2(b) shows that the surface scale is significantly thinner after step 2 than after step 1. This oxide removal goes with a mass loss [9]. Also, the chromium and manganese fractions in the remaining oxide have decreased while the aluminium fraction has dramatically increased [7].

Moreover, carbon profiles by GDOES (Fig. 3) show a clear decrease of the carbon content in the vicinity of the alloy surface after step 2.

The following evidence (i) the removal of the surface chromia, (ii) the removal of dissolved carbon, and (iii) the CO(g) production, leads to the assumption that chromia reacts with carbon from the alloy to produce CO(g) and metallic chromium according to:

$$Cr_2O_{3(s)} + 3C_{(s)} \overset{T>T_a}{\rightarrow} 3CO_{(g)} + 2Cr_{(s)} \quad (7)$$

Eq. (7) was proposed by Brenner and Graham [22], Quadakkers and Schuster [21,25,30], Warren [24], and Christ et al. [26] for Alloy 617. Model alloys with or without carbon were used to prove that the previous scheme actually takes place in impure helium [11]. A test was also performed under helium without carbon monoxide or methane; Eq. (7) happened to occur anyway. Cr-rich oxide rapidly reacts: in test He-1, the entire Cr-rich layer has been removed within 20 h at 1253 K; depending on kinetics, Mn-rich oxide can also be

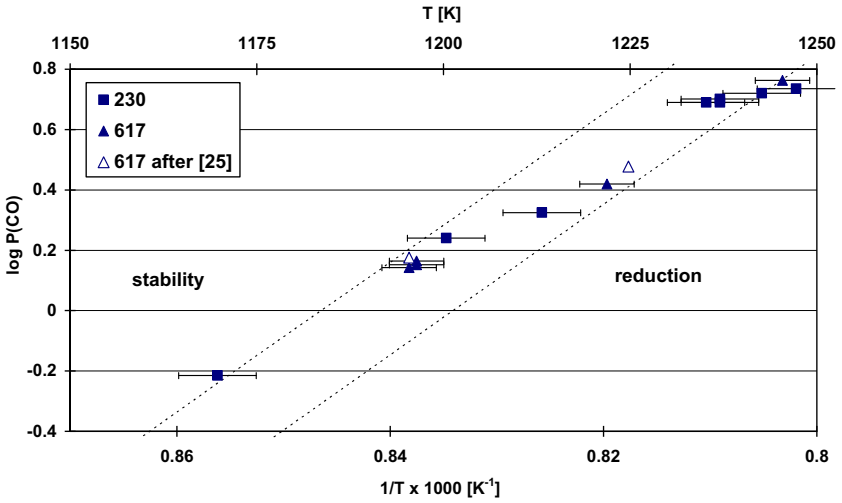

Fig. 4. Critical temperature T_A in impure helium versus P(CO) after Table 2 and Ref. [9]; published data for Alloy 617 from Ref. [27] in helium containing 50 Pa H_2, 2.2 Pa CH_4 and ~0.05 Pa H_2O.

fully reduced. However, Al-rich oxide is thermodynamically stable versus Eq. (7) [8]. Brenner [22] assumed that Eq. (7) involves gaseous intermediates such as CO(g) and CO_2(g) that will exist within a 'microclimate' at the alloy/chromia vicinity. As was already discussed by Christ et al. [26], Rouillard et al. [8,10] has shown that Eq. (7) can proceed without any gaseous intermediates. It is thus proposed that chromia reduction could be a direct solid/solid reaction that will take place at the alloy/chromia interface. This assumption implies that CO(g) should be transported from the inner interface to the gas phase through the scale [10].

4.3. Influence of the helium chemistry

According to Brenner's terminology [22], the critical temperature at the beginning of the steep CO(g) peak in Fig. 1 is called T_A. T_A was determined in the various test gas mixtures He-1 to He-5 and the experimental values, given in Table 2, change from 1168 to 1242 ± 5 K. Fig. 4 from Table 2 and Ref. [9] plots the evolutions of T_A versus P(CO) for Alloys 617 and 230. It clearly appears that the higher the partial pressure of carbon monoxide, the higher T_A. Data for the two alloys fall within the same scatter band. Quadakkers [25] has proposed that T_A could be the equilibrium temperature of Eq. (7). Using this approach, a comprehensive model was developed in Ref. [10] to assess T_A to P(CO). The model highlights that, as Eq. (7) occurs at the alloy/chromia interface, it is relevant to use local thermodynamic values such as interfacial chromium activity and interfacial carbon activity.

5. Corrosion behavior of Ni-base alloys in coolant helium at 1223 K

The previous section emphasized that chromia-forming alloys react in impure helium following two main modes, depending on the temperature and the carbon monoxide partial pressure in the gas phase. In Fig. 4, the area located at intermediate temperatures and higher carbon monoxide partial pressures will induce oxidation of chromium into chromia while the area above the curve at higher temperature and lower P(CO) corresponds to instability of the surface chromia because it is irreversibly reduced by the carbon from the alloy. In the following, the corrosion behavior of IHX candidate alloys, Alloy 617 and Alloy 230, will be investigated at 1223 K for exposures up to 5000 h in impure helium. Composition of the test gasses is established according to Fig. 4: some helium mixtures (He-9), called 'oxidizing' helium, should promote chromia and others (He-10 to He-12) falling within the area that destabilizes the chromium oxide are called 'reducing' conditions. In order to address the effect of methane and vapor, various P(CH_4) and P(H_2O) were tested.

5.1. Behavior of Ni-base alloys in 'oxidizing' helium

Fig. 5(a) and (b) show SEM cross-sections respectively of Alloy 230 and Alloy 617 tested for 813 h at 1223 K in 'oxidizing' helium He-9. As expected in the oxidizing conditions, alloys exhibit a surface scale that is made of chromium-rich oxide.

Main corrosion features are: (i) growth of the chromia scale, (ii) internal oxidation of aluminium, (iii) slight increase in carbon content, and (iv) development of a carbide-free zone.

(i) As shown in Section 4.1 after a couple of hours, the reaction of CO(g) following Eq. (3) becomes negligible and water vapor is the only oxidant of importance. Eq. (1) thus prevails and chromium oxidizes into chromia; other minor oxidizable elements react as well. Long duration tests in impure 'oxidizing' helium show that specimens still exhibit a surface oxide after 5000 h. This means that oxidation is a sustainable behavior for at least 5000 h. As exemplified in Fig. 6, all specimens gain mass in these conditions. Moreover, the longer the exposure, the higher the mass gain and the thicker the surface scale [4] in agreement with parabolic kinetics limited by diffusion phenomena throughout the scale as observed by Cook et al. [31] for Alloy 617. Although Fig. 6 only reports few data, an approximate parabolic rate constant was tentatively assessed for Alloy 230; $k_p \approx 1.1 \times 10^{-13}\ g^2\ cm^{-4}\ s^{-1}$.

Alloy 230 exhibits lower oxidation rate than Alloy 617 (see the smaller mass gains in Fig. 6). This slower oxidation can be ascribed to both a thinner surface scale and less internal oxidation. Scale growth kinetics is influenced by incorporation of minor elements in the surface chromia. In the case of Alloy 230, manganese exhibits a strong tendency to concentrate in the outer zone of the scale, in relation to a diffusion coefficient hundred times larger than that of chromium itself in Cr_2O_3 at 1223 K [32] and tends to form a spinel phase with chromium in the outer part of the scale. In the development of Hastelloy XR, Shindo and Kondo [33] claimed that adding manganese to Hastelloy X enhanced resistance to oxidation

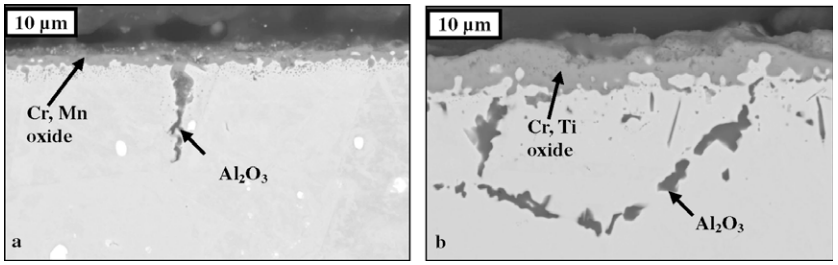

Fig. 5. SEM images with backscattered electron contrast at 20 kV – Cross section of the surface of Alloy 230 (a) and Alloy 617 (b) after 813 h at 1223 K in He-9.

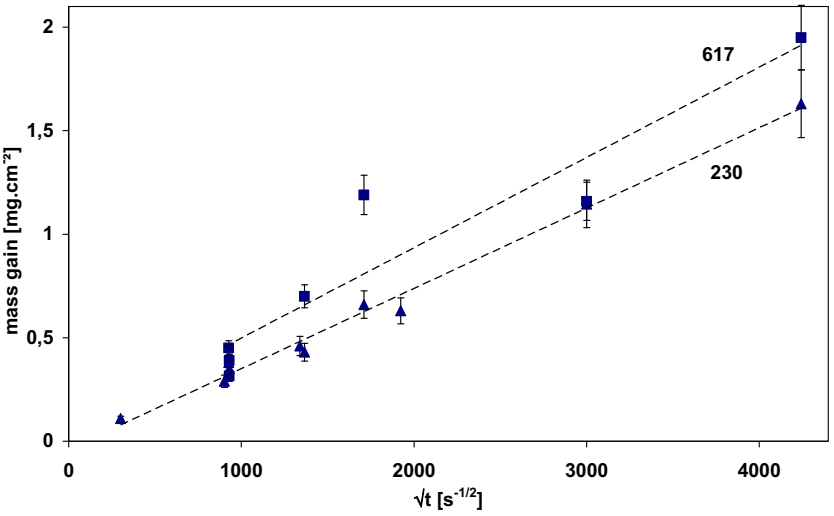

Fig. 6. Mass gains of Alloy 617 and Alloy 230 after exposures at 1223 K in He-9 versus square root of time; parabolic oxidation rate constant is approx. $k_p \approx 1.1 \times 10^{-13}$ g^2 cm^{-4} s^{-1} for Alloy 230.

of chromium. For Alloy 617, the surface chromia contains titanium [4,6].

(i) Some internal oxides containing Al, Ti or Si are also evident close to the oxide/alloy interface. These nodules may have formed at the very beginning of the oxidation test [8] and grew because the oxygen pressure prevailing at the alloy/chromia interface (set by the dissociation of chromia) enables them to be oxidized. However, minor Si and Al should stop reacting because of their progressive depletion in the surface vicinity. Aluminium oxide is formed deeper in the alloy. Internal oxidation is observed at grain boundaries in Alloy 230 (as grain boundaries represent high diffusion paths) but is intergranular and intragranular in Alloy 617. It is deeper and more intense when the test time increases. Cook and Graham [34] has shown that the degree of internal oxidation of Alloy 800H decreases with reduction in the alloy Al content. The higher oxidation rate of Alloy 617 may thus be partly due to its rather high aluminium content that promotes internal oxidation.

(ii) Table 3 gives the total carbon content measured by the LECO analyzer in 2 mm-thick specimens exposed for 500 h in various test helium mixtures. The carbon weight percentage has slightly increased after treatment in 'oxidizing' helium. An increase in carbon corresponds to a deposition in the alloy by carbon-bearing gasses CO(g) or CH_4(g). The environment is actually carburising towards the structural alloys [30] but the formation of the surface oxide effectively minimises the carburization by forming a barrier between the gas and the metal. In the case of 'oxidizing' helium, limited reactivity of carbon monoxide and methane according to Eqs. (3) and (4) is thus observed.

As the surface chromia scale effectively protects the surface from exchange with the gas phase, the inner composition and microstructure of alloys do not significantly change. The bulk properties, such as tensile and creep strengths, are thus expected to be maintained [27].

(i) Beneath the growing oxide scale, a carbide-free zone develops: due to thermal ageing (see Section 3.1), significant precipitation of secondary carbides – mainly of the $M_{23}C_6$ type and rich in Cr – occurs in the alloy bulk at grain boundaries after treatment at 1223 K; but these secondary intergranular carbides do not form in a sub-surface zone which penetrates somewhat deeper than the internal oxidation. It was shown that the depth of this zone is related to the chromia thickness [4]. One possible cause could be the depletion of Cr in the sub-surface zone leading to increased solubility of carbon in the depleted substrate.

5.2. Behavior of Ni-base alloys in 'reducing and decarburizing' helium

Fig. 7 shows cross-section pictures of Alloy 230 at 1223 K in test helium He-10 that falls within the area for chromia instability (P(CO) = 0.5 Pa in Fig. 4) and without methane. As expected in the 'reducing' conditions, alloys do not exhibit any surface oxide.

Table 3
Global carbon weight percentage analyzed by LECO in as-received and corroded alloys (exposed for 500 h at 1223 K in He-9 to He-12) and specimen thickness.

	as-received	He-9	He-10	He-11	He-12
Alloy 230	0.101 ± 0.05	0.075 ± 0.03 wt% C (δ = 0.87 mm)	0.075 ± 0.03 wt% C (δ = 1.96 mm)	0.170 ± 0.08 wt% C (δ = 1.75 mm)	1.78 ± 0.90 wt% C (δ = 1.46 mm)
Alloy 617	0.067 ± 0.03	0.097 ± 0.02 wt% C (δ = 0.81 mm)	0.035 ± 0.02 wt% C (δ = 2.00 mm)		0.56 ± 0.20 wt% C (δ = 1.44 mm)

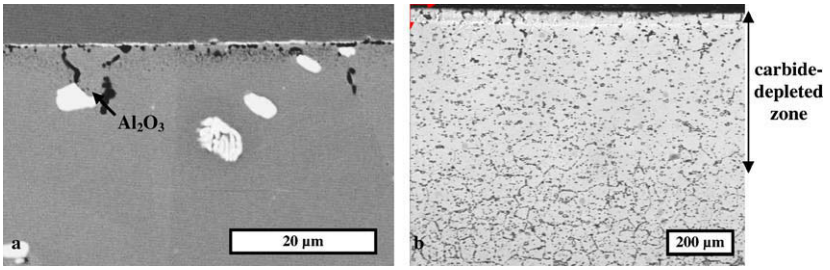

Fig. 7. Alloy 230 surface after exposure at 1223 K in He-10; (a) SEM image with a backscattered electron contrast at 20 kV after 240 h, and (b) micrograph after 1000 h.

Main corrosion features are: (i) absence of chromia scale, (ii) internal oxidation of aluminium, (iii) decrease of the carbon content, and (iv) dissolution of primary carbides and development of a deep secondary carbide-free zone.

(i) Due to reduced P(CO) in the test gas He-9, Eq. (7) is driven to the right hand side. Cr-rich oxide is then reduced by the carbon from the alloy to release some chromium. In the mean time, water vapor can still react with reactive elements, first of all Cr, following Eq. (1). This regenerates surface chromia and sustains the corrosion. It is worth noticing that a kinetic competition occurs between Eqs. (1) and (7). The relative reaction rates, depending on environmental factors, such as temperature and $P(H_2O)$, determine whether Cr_2O_3 is fully removed from the surface as in Fig. 7(a) [Eq. (7) plus possibly Eq. (2) faster than Eq. (1)] or not [Eq. (1) faster than Eq. (7)]. In this later case, a highly porous chromia scale is formed on the surface [22] that is totally pervious to gas transport toward the alloy.
(ii) As already mentioned, Eq. (7) does not affect Al or Si oxide and internal oxidation of Al thus proceeds.
(iii) System of Eqs. (1) and (7) leads to consumption of the dissolved carbon that is removed from the alloy surface in the form of CO(g). Table 3 shows that within 500 h at 1173 K, Alloy 617 has lost about 50% of its initial carbon.
(iv) Carbon will thus diffuse from the bulk to the surface. Along the concentration gradient, carbides are destabilized as shown by the global process:

$$\text{carbides} \rightarrow C_{(s)} + M_{(s)} \tag{8}$$

Degree of dissolution will depend on the carbide stability as well as kinetic factors. Fig. 7(b) shows partial dissolution of primary carbides in the surface vicinity as well as a deep zone free of secondary carbides. The global carbon loss as well as the depth of the carbide-free zone increased with exposure time.

It is expected that dissolution of secondary carbides, which participate in the alloy strengthening at high temperature by limiting the grain boundary glide, will have a dramatic effect on the creep rupture life [35].

5.3. Behavior of Ni-base alloys in 'reducing and carburizing' helium

He-11 and He-12 contain 0.5 Pa and 1.5 Pa carbon monoxide, and 2 and 30 Pa methane. According to Fig. 4, both conditions should be reducing toward chromia. Exposure to these test gasses has produced carburization of chromia forming alloys. Fig. 8(a) and (b) show SEM cross-section pictures of Alloy 230 and Alloy 617 after 240 h at 1223 K in the highly carburizing conditions.

Main corrosion features are: (i) absence of chromia scale, (ii) internal oxidation of aluminium, (iii) increase of the carbon content, and (iv) precipitation of surface and internal carbides.

(i) As expected in the 'reducing' conditions, Eq. (7) is initiated and surface chromia is unstable versus dissolved carbon. As explained in Section 4.2, Eq. (1) can still proceed, regenerating surface chromia and causes internal oxidation of aluminium.
(ii) In the mean time cracking of methane on the alloy – following Eq. (4) – deposits carbon on the surface. Part of the carbon can in turn participate to the chromia reduction.
(iii) Carbon excess will either precipitate on the surface or diffuse into the bulk.
(iv) As carbon diffuses deep into the alloy, the local carbon solubility limit is reached and coarse internal carbides can be formed, following the global process:

$$C_{(s)} + \text{metal} \rightarrow \text{carbides} \tag{9}$$

In Fig. 8(a) and (b) surface carbides as well as coarse inter- and intra-granular carbides have formed. The front of coarse carbides goes deeper in the bulk when exposure time increases. XRD analysis indicates that carbides are mainly of the Cr_2C_3 and $Cr_{23}C_6$ types. In addition, Table 3 shows an increase in the global carbon concentration of alloys after exposure to test gasses He-11 and He-12. The alloys took less carbon up after exposure to He-11 than to He-12. And, the alloys took more carbon up when the exposure time was longer.

Precipitation of coarse internal carbides is known to be associated with low temperature embrittlement of metallic materials. Ennis et al. [36] has shown a dramatic decrease in the room temperature impact energy, the tensile strength, and the rupture elongation of carburised Alloy 617. Increase of 0.4% of the carbon content induces full embrittlement of the alloy.

Kinetic competition between Eqs. (1), (4), and (7) determines the quantities of oxygen and carbon which are transferred to/from the alloy. Increasing methane content in the gas phase from 0 (He-10) to 2 Pa (He-11) changes the corrosion behavior from decarburization to carburization; further increase in the $P(CH_4)$ to 30 Pa (He-12) has a strong influence on the intensity of carburization as

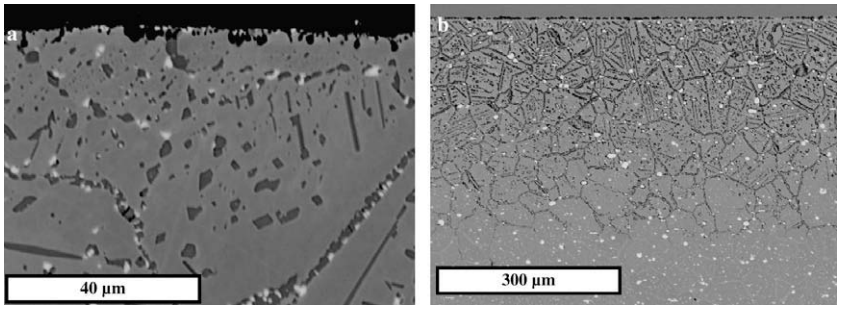

Fig. 8. SEM images with backscattered electron contrast at 20 kV of the surface of Alloy 617 (a) and Alloy 230 (b) after 240 h at 1223 K in He-12.

CH_4 cracking transfers carbon to the alloy. Brenner [22] assumed that a critical CH_4/H_2O ratio determines whether the substrate will be decarburised or carburised. Quaddakers [30] tentatively measured this ratio for Alloy 617 at 1223 K and proposed a value of 100/1 (if the CH_4/H_2O ratio exceeds 100/1, helium would be carburising). Results obtained in methane-free versus methane-containing test gasses globally agree with this prediction although the value of the critical ratio should be accurately assessed.

Mention should be made of the ability for Alloy 617 to form alumina scales in very dry conditions [23]. This has been observed in 'reducing' helium with low water vapor content [6]. Under these circumstances chromia can not form; instead aluminium oxidizes at the surface to form a thin film of Al_2O_3 following Eq. (1). The presence of this film prevents internal oxidation, as well as decarburization and carburization. As already discussed by Graham [12], this specific behavior cannot be a reliable technological solution to the prevention of corrosion in HTR systems. It is actually considered that the water vapor level during reactor start-up would always leads to the formation of a chromia-based surface layer and consumption of the aluminium reservoir by internal oxidation.

6. Conclusion

HTR helium coolant is expected to contain impurities which can interact with metallic materials at high temperature, especially with structural chromia-forming nickel base alloys. Interplay between the alloy surface, temperature, and gas composition determines whether corrosive oxidation, carburization, or decarburization occurs. Corrosion phenomena which significantly impact the mechanical stability are carburization – associated with low temperature embrittlement and decarburization – causing a reduced creep rupture life. Within the primary circuit of the reactor, the environment must always sustain chromium oxidation, because a continuous, self-healing, chromia-based surface scale is needed to act as a barrier against the reactive gasses. However, a specific process occurs at high temperature which irreversibly reduces chromia; this reaction can be suppressed by increasing the CO partial pressure. A first approach that must be considered to mitigate high temperature corrosion of circuit and heat exchanger alloys is thus the control of the helium chemistry, especially in terms of CO partial pressure. However, the atmosphere must also be compatible with other high temperature materials in particular, carbon-base in-core structures.

Regarding the alloy chemical composition, manganese may lower the chromia growth rate whereas aluminium induces internal oxidation. As was previously performed for Hastelloy X in Japan, optimisation of the alloy chemistry within the specification could limit the oxidation rate.

Acknowledgments

The material program was being performed in cooperation with AREVA NP and EDF and the author is especially grateful to P. Combrade, G. Girardin, J. Chapovaloff of AREVA NP and M. Blat of EDF R&D. Contribution to this work of F. Rouillard, B. Duprey, C. Desgranes, S. Guillou, A. Monnier, P. Lett, F. Thieblemont, A. Thomazic, L. Lemort; M. Tabarant (CEA, DEN, DPC, SCP); H. Burlet, J. M. Gentzbittel and L. Guétaz (CEA, DRT, LITEN); K. Wolski (Ecole Nationale Supérieure des Mines SE) is greatly acknowledged.

References

[1] A Technology Roadmap for Generation IV Nuclear Energy Systems, Report GIF002-00, US Department of Energy/Generation IV International Forum, 2002.
[2] J.-C. Gauthier, G. Brinkmann, B. Copsey, M. Lecomte, Nucl. Eng. Des. 236 (2006) 526.
[3] T.R. Allen, K. Sridharan, L. Tan, et al., Nucl. Technol. 162 (2008) 342.
[4] C. Cabet, A. Terlain, P. Lett, et al., Mater. Corr. 57 (2006) 147.
[5] C. Cabet, F. Rouillard, B. Duprey, in: Structural Materials for Innovative Nuclear Systems (SMINS), OECD Publishing, London, 2008.
[6] C. Cabet, F. Rouillard, B. Duprey, in: Proceedings of EUROCORR'2007, Freiburg iB, Germany, 2007.
[7] F. Rouillard, C. Cabet, K. Wolski, et al., J. Nucl. Mater. 362 (2007) 248.
[8] F. Rouillard, C. Cabet, K. Wolski, M. Pijolat, Oxid. Met. 68 (2007) 133.
[9] C. Cabet, J. Chapovaloff, F. Rouillard, et al., J. Nucl. Mater. 375 (2008) 173.
[10] F. Rouillard, C. Cabet, S. Gossé, et al., Mater. Sci. Forum. 595–598 (2008) 429.
[11] C. Cabet, G. Girardin, F. Rouillard, et al., Mater. Sci. Forum. 595–598 (2008) 439.
[12] L.W. Graham, J. Nucl. Mater. 171 (1990) 76.
[13] T. Kondo, Gas-Cooled Reactors Today, vol. 4, BNES, London, 1983, p. 153.
[14] H. Nickel, F. Schubert, H. Schuster, Nucl. Eng. Des. 78 (1984) 251.
[15] H. Burlet, J.M. Gentzbittel, C. Cabet, et al., in: Structural Materials for Innovative Nuclear Systems (SMINS), OECD Publishing, London, 2008.
[16] L.W. Graham, M.R. Everett, D. Lupton, et al., Gas-Cooled Reactors with Emphasis on Advanced Systems, vol. I, IAEA, Vienna, 1976, p. 319.
[17] K. Krompholz, J. Ebberink, G. Menken, Proceedings of 8th International Congress on Metallic Corrosion, vol. II, Dechema, Frankfurt, 1981, p. 1613.
[18] R. Nieder, Proceedings of Gas-Cooled Reactors Today, vol.2, BNES, London, 1982, p. 91.
[19] G.E. Wasielewski, A.M. Beltran, H.M. Fox, F.E. Sczerzenie, in: Proceedings of Jülich Symposium on Gas-Cooled Reactors with Emphasis on Advanced Systems, vol. I, Paper No. IAEA-SM200/56, IAEA, Vienna, 1976, p. 379.
[20] N. Sakaba, Y. Hirayama, in: Proceedings of GLOBAL 2005, Paper No. 263, Tsukuba, Japan, 2005.
[21] W.J. Quadakkers, H. Schuster, Nucl. Technol. 66 (1984) 383.
[22] K.G.E. Brenner, L.W. Graham, Nucl. Technol. 66 (1984) 404.
[23] G. Menken, R. Nieder, W.L. Graham, et al., Gas-Cooled Reactors Today, vol. 2, BNES, London, 1982, p. 185.
[24] M.R. Warren, High Temp. Technol. 4 (1986) 119.
[25] W.J. Quadakkers, Werkstoffe und Korrosion 36 (1985) 335.
[26] H.J. Christ, U. Künecke, K. Meyer, H.G. Sockel, Mater. Sci. Eng. 87 (1987) 161.
[27] M. Shindo, W.J. Quadakkers, H. Schuster, J. Nucl. Mater. 140 (1986) 94.
[28] J. Chapovaloff, D. Kaczorowski, G. Girardin, Mater. Corros. 59 (2008) 584.
[29] G. Girardin, Technical Center, AREVA NP, Private Communication.
[30] W.J. Quadakkers, H. Schuster, Werkstoffe und Korrosion 36 (1985) 141.
[31] R.H. Cook, R. Exner, L.W. Graham, in: Proceedings of Specialists' Meeting on High-Temperature Metallic Materials for Gas-Cooled Reactors, Cracow, Poland, 1988, p. 129.
[32] R.E. Lobnig, H.P. Schmidt, K. Hennesen, et al., Oxid. Met. 37 (1&2) (1992) 81.
[33] M. Shindo, T. Kondo, Nucl. Technol. 66 (1984) 429.
[34] R.H. Cook, L.W. Graham, in: W. Betteridge et al. (eds.), Chemical Behavior and Mechanical Performance in HTR-Helium at High Temperatures in Alloy 800, Netherlands, 1978, p. 309.
[35] Y. Kurata, Y. Ogawa, H. Nakajima, T. Kondo, in: Proceedings of workshop on structural design criteria for HTR, Jülich, Germany, 1989, p. 275.
[36] P.J. Ennis, K.P. Mohr, H. Schuster, Nucl. Technol. 66 (1984) 363.